doi:10.3772/j.issn.1006-6748.2018.01.003

Abnormal driving behavior identification based on direction and position offsets①

Zhang Xiaorui(张小瑞)②[*,***], Sun Wei[**,***], Xu Ziqian[*], Yang Cuifang[**], Liu Xinzhu[*]
([*]Jiangsu Engineering Center of Network Monitoring, Nanjing University of Information Science & Technology, Nanjing 210044, P.R.China)
([**]School of Information and Control, Nanjing University of Information Science & Technology, Nanjing 210044, P.R.China)
([***]Jiangsu Collaborative Innovation Center on Atmospheric Environment and Equipment Technology, Nanjing University of Information Science & Technology, Nanjing 210044, P.R.China)

Abstract

Abnormal driving behavior identification (ADBI) has become a research hotspot because of its significance in driver assistance systems. However, current methods still have some limitations in terms of accuracy and reliability under severe traffic scenes. This paper proposes a new ADBI method based on direction and position offsets, where a two-factor identification strategy is proposed to improve the accuracy and reliability of ADBI. Self-adaptive edge detection based on Sobel operator is used to extract edge information of lanes. In order to enhance the efficiency and reliability of lane detection, an improved lane detection algorithm is proposed, where a Hough transform based on local search scope is employed to quickly detect the lane, and a validation scheme based on priori information is proposed to further verify the detected lane. Experimental results under various complex road conditions demonstrate the validity of the proposed ADBI.

Key words: abnormal driving behavior identification(ADBI), lane detection, vanishing point detection, improved Hough transform

0 Introduction

With the rapid increase of vehicle amount, traffic accidents have become serious problems in China. It was reported that in China 274 persons died from abnormal driving in 2015, which accounted for 8.9% of the death in traffic accidents. According to the information provided by the traffic management bureau, about 40% fateful traffic accidents result from abnormal driving such as fatigue driving and illegal lane change. Thus, the research on the abnormal driving behavior identification (ADBI) of drivers is of very important practical significance.

Currently, there are mainly three kinds of ways to identify abnormal driving behaviors: (1) identification based on physiological characteristics. (2) identification based on facial characteristics. (3) identification based on vehicle behavior characteristics. The identification based on physiological characteristic detects drivers' electroencephalogram (EEG) and electrocardiograph (ECG) directly[1,2] has high reliability. However, the detection equipment used in this method is directly connected to drivers' skin, which will more or less disturb drivers during the long driving period. The identification based on facial characteristic extracts the drivers' facial characteristics in real time by a camera, such as blink frequency[3], to analyze driver's abnormal driving behavior. Nevertheless, this kind of method has high error rate when a driver wears a pair of glasses[4]. The identification based on vehicle behavior characteristics detects driver's driving behavior according to the output performance of the operated vehicle, such as the variation of steering wheel angle[5,6]. By using this method, some interference such as illumination change can be avoided, but the method is easily affected by driver's driving habit. In conclusion, although these methods above can achieve the goal of identifying driver's abnormal driving behavior, they still have some limitations in terms of accuracy and reliability under complex road environment.

In order to deal with the limitations of the existing

① Supported by the National Natural Science Foundation of China (No. 61304205, 61502240), Natural Science Foundation of Jiangsu Province (BK20141002) and Innovation and Entrepreneurship Training Project of College Students (No. 201710300051, 201710300050) and Foundation for Excellent Undergraduate Dissertation (Design) of Naning University of Information Science & Technology.

② To whom correspondence should be addressed. E-mail: zxr365@126.com

Received on Sep. 10, 2017

methods, a new ADBI method based on lane and vanishing point detection is proposed and the lane image is preprocessed firstly by using a gradient enhancement method based on linear discriminate analysis (LDA) and the edge detection algorithm based on Sobel operator and adaptive threshold segmentation to enhance the lane edge. After selecting a region of interest, the lane is extracted by a Hough transform based on local research scope by setting constraint to polar radius and polar angle, which can improve the efficiency of the lane extraction. Then, an algorithm based on a scanning algorithm according to the brightness differences between the lanes and the roads is used to further verify the detected lanes. Finally, a new ADBI method based on the offset angle and lateral distance is proposed to judge whether the abnormal driving behavior occurs. The whole process of the ADBI is shown in Fig. 1.

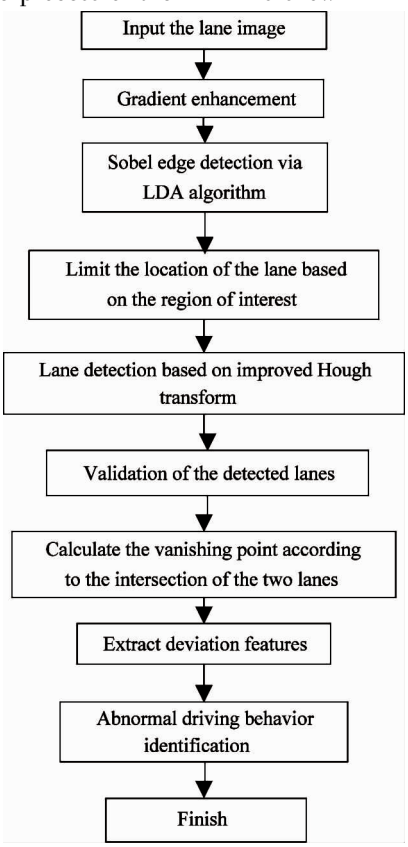

Fig. 1 The flow chart of ADBI

The contributions of the paper are as follows. (i) A new ADBI method is proposed, where both direction and position offsets are together considered as identification condition. Compared with state-of-the-art methods, which typically consider only one aspect of direction and position offsets during ADBI, the proposed method can improve the accuracy and reliability of the ADBI due to considering two aspects of abnormal driving. (ii) A validation scheme based on priori information is proposed to further verify the detected lane, which can effectively eliminate some typical interference factors, e. g., road edge and highway barrier edge, and improve reliability of lane detection.

1 Image preprocessing

In order to filter noises and enhance the lane edge, image preprocessing should be done firstly, which will simplify the following processing steps and improve real-time performance.

1.1 Gradient enhancement based on LDA

Color is an unstable characteristic which can be easily affected by the change of illumination. If the illumination is poor, it will become difficult to distinguish the lanes from the roads. Thus, in this work, a gradient enhancement method based on LDA is proposed in order to generate optimal RGB weights and enhance the edge of lanes:

(1) Definition of lane gradient is as follows[7]:

$$g_l = | W \cdot X^l - W \cdot X^r | \tag{1}$$

where W is a conversion vector which converts the color image into the gradient-enhanced image, and X^l and X^r are the RGB pixel values of the lane region and the road respectively.

(2) The key to gradient-enhancing conversion is to find vector $W_{\max}$ which satisfies the following equation:

$$\begin{aligned} g_l(W_{\max}) &= \max(g_l(w)) \\ &= \max | W \cdot X^l - W \cdot X^r | \end{aligned} \tag{2}$$

(3) In order to figure out X^l and X^r, training data which consist of road and lane classes are needed. Training data for class c for the frame at time t are defined as follows:

$$T_c^t = \{ X_c^{t-k}, X_c^{t-(k-1)}, X_c^{t-(k-2)}, \cdots, X_c^{t-1} \} \tag{3}$$

where T_c^t denotes training data of class c for the t^{th} frame at time, c represents either the lane or the road, X_c^t denotes training data for class c extracted from the t^{th} frame, and k is the number of previous frames to be used as training data for the current frame.

(4) To find $W_{\max}$ in Eq. (2), the vector that can maximize discriminance between the two classes (lane class and road class) should be figured out, and this problem can be solved by LDA. LDA is used to find a linear combination of between-class scatter S_B and within-class scatter S_W. The definitions are as follows:

$$\begin{aligned} S_B &= \sum_{i=1}^{c} n_i (m_i - m)(m_i - m)^{\mathrm{T}} \\ S_W &= \sum_{i=1}^{c} \sum_{x \in C_i} n_i (x - m)(x - m)^{\mathrm{T}} \end{aligned} \tag{4}$$

where x is data, n_i is the amount of data in class i, m_i denotes the mean of class i, m is the mean of all data, c is the number of classes, and C_i denotes a set of all data in class i.

(5) By minimizing the within-class-scatter and maximizing the between-class-scatter, the lane class and the road class can be distinguished from each other. Thus,

$$W_{\max} = \arg\max | W^{\mathrm{T}} S_B W / W^{\mathrm{T}} S_W W | \quad (5)$$

(6) Finally, the image after gray-level conversion can be calculated:

$$I' = W_{\max} \cdot I \quad (6)$$

where I is RGB value of the original image, and I' is the image after gradient enhancement.

1.2 Edge detection based on Sobel adaptive algorithm

After the gradient enhancement, the lanes become more noticeable and easy to be distinguished. Based on the gradient-enhanced images, the edge detection via Sobel adaptive algorithm is used to extract the edge points of the lanes for the following lane detection.

By edge detection, edge information can be retained and the amount of data processing is reduced. Thus, self-adaptive threshold Sobel algorithm is used to extract the edge information of lanes.

The Sobel operator in x and y directions can be represented as[7]:

$$S_x = \begin{bmatrix} -1 & -2 & -1 \\ 0 & 0 & 0 \\ 1 & 2 & 1 \end{bmatrix} \quad S_y = \begin{bmatrix} 1 & 2 & 1 \\ 0 & 0 & 0 \\ -1 & -2 & -1 \end{bmatrix} \quad (7)$$

Assume that G_x and G_y are the horizontal and vertical gradient values of the image, then:

$$G_x = S_x \times I', \ G_y = S_y \times I' \quad (8)$$

And the gradient value of the pixel whose coordinates are (x, y) can be figured out:

$$G = \sqrt{G_x^2 + G_y^2} \quad (9)$$

Unlike classical Sobel algorithm which requires constant thresholds, a self-adaptive edge detection algorithm is used in the paper. The Canny edge detector uses two threshold values to determine edges. Pixels with gradient values above the larger threshold T_l are selected as edges. On the other hand, pixels with values below the smaller threshold T_s are determined as non-edges. Pixels between the two thresholds are set as edge candidates and are classified as edges if there is a path from the pixel to an edge. After gradient enhancement, the RGB vectors of the lanes and roads are normally distributed[8]. Therefore, these adaptive thresholds can be self-adaptively calculated from statistical characteristics of the road and lane class. Large threshold value T_l can be determined by

$$T_l = | W_{\max} \cdot m^l - W_{\max} \cdot m^r | \quad (10)$$

where m^l and m^r are the mean RGB values of the lane region and the road region respectively.

Small threshold value T_s is determined by

$$T_s = \max(| W_{\max} \cdot m^l - d |, | W_{\max} \cdot m^r - d |) \quad (11)$$

where d is a value for which lane and road probabilities are equal[9].

2 Detection of lane and vanishing point

2.1 Selection of region of interest

Generally, useful lane information is mainly at the bottom of the road image. Thus, the bottom part of the captured image is determined as the region of interest to reduce the calculation amount of lane detection. In order to detect the two lanes in both sides of the vehicle, the region of interest is further divided into two parts, denoted as R_L and R_R respectively. The following steps are all implemented in the region of interest. The partition of lane image is shown in Fig. 2.

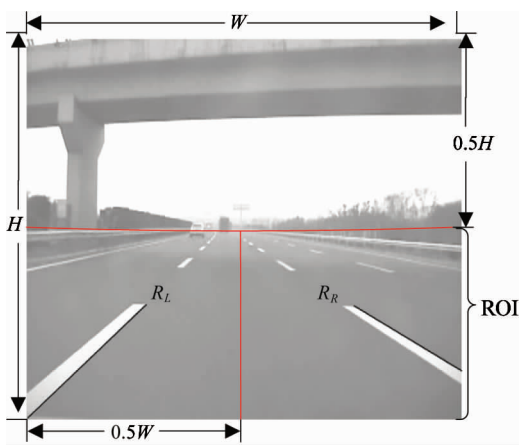

Fig. 2 Partition of lane image

2.2 Lane detection

Traditional Hough transform lane detection algorithms are based on a huge search scope. As a result, the calculation is time-consuming and these algorithms are not suitable for real-time online detection. Therefore, an improved Hough transform is used to improve the efficiency of the edge detection. By setting constraint to polar angle and polar radius, the search scope of the Hough transform is greatly shrunken.

Assuming that in the t^{th} frame, the polar radiuses of the lanes on both sides of the vehicle are ρ_l^t and ρ_r^t, and polar angles of that are θ_l^t and θ_r^t respectively. The

experiments on a video involving a large amount of lane images[10,11] show that the lane in the t^{th} frame is just adjacent to the lane in the $(t+1)^{th}$ frame in spatial location.

Thus, if the search scope for Hough transform is limited in the area adjacent to the lane in the t^{th} frame before using Hough transform[11] to extract polar radius ρ_l^{t+1} and ρ_r^{t+1} as well as polar angle θ_l^{t+1} and θ_r^{t+1} in $(t+1)^{th}$ frame, the computational burden of the Hough transform will be greatly reduced, and the efficiency of the lane detection based on the Hough transform will be improved as well.

Therefore, in this paper, the lane is detected by the improved Hough transform algorithm based on local search scope. The search scope of polar radiuses and polar angles in the $(t+1)^{th}$ frame based on the detected polar radiuses and polar angles in the t^{th} frame is determined as: $\rho_l^t - \alpha \leqslant \rho_l^{t+1} \leqslant \rho_l^t + \alpha$, $\rho_r^t - \alpha \leqslant \rho_r^{t+1} \leqslant \rho_r^t + \alpha$, $\theta_l^t - \varepsilon \leqslant \theta_l^{t+1} \leqslant \theta_l^t + \varepsilon$, $\theta_r^t - \varepsilon \leqslant \theta_r^{t+1} \leqslant \theta_r^t + \varepsilon$, where α and ε are two threshold values. In the paper, we let $\alpha = 15$, $\varepsilon = 10$ to obtain an high-efficiency detection.

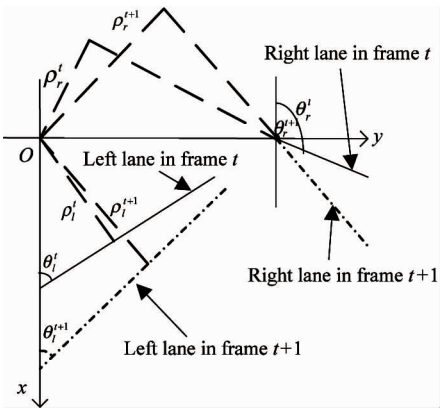

Fig. 3 Constraint of lane domain

Based on the research scope determined above, we can obtain the two parameters of the detected lane using the Hough transform[7], that is, ρ and θ, where ρ and θ express polar radius and polar angle in polar coordinate system respectively. From Fig. 3, the inclination angle θ' of a line in Cartesian coordinate system can be described as

$$\theta' = 90° - \theta \tag{12}$$

2.3 Validation of the detected lanes

So far, the lanes have been preliminarily detected. However, in some cases, the detected lanes could not be real ones due to the distraction from other edge lines in the image, such as the edge of the road or highway barrier. Therefore, we need to further verify the detected lanes.

An existing study[12] finds that the lane region is generally much brighter than the surrounding regions on both sides of it, so its gray-level value is obviously higher than that of the surrounding areas. Based on the priori information in structure and brightness, we formulate a set of rules to verify the detected lane. The formulated rules are as follows:

(1) Three 4×24 windows side by side are named A, B and C. The gray average of the pixels in each window is denoted by m_A, m_B and m_C, respectively. Based on the analysis above, if there is a real lane across region B, such as $A_1B_1C_1$ in Fig. 4, then three gray averages of three windows will satisfy the following inequation[13]:

$$\begin{cases} m_B - m_A > 20 \\ m_B - m_C > 20 \end{cases} \tag{13}$$

If there is an unreal lane across region B, such as $A_2B_2C_2$ in Fig. 4, then three gray averages of three windows will not satisfy the inequation (13).

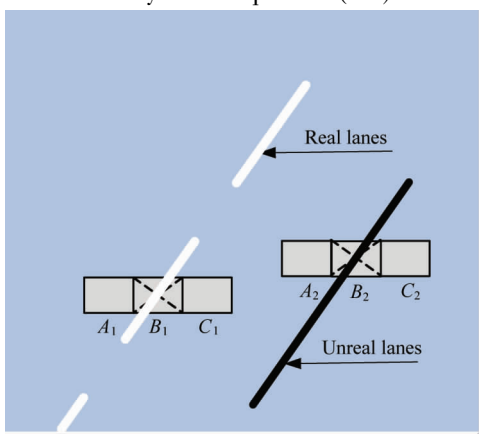

Fig. 4 Schematic diagram of validation of the detected lanes

(2) When the lane is blocked by other vehicles or becomes blurred, the lane might be not continuous. Therefore, it is impossible for every pixel in the real lane to satisfy in inequation (13). In order to enhance the robustness of lane validation, a constraint is set as

$$\frac{N_S}{N_T} > \tau_T \tag{14}$$

where N_S denotes the number of pixels that satisfy the inequation(13), N_T denotes the total number of pixels on the detected lane, τ_T is a threshold value. Based on plenty of field experiments, when $\tau_T = 0.19$, best detection results can be obtained.

If the grey values of pixels in the detected lane meet the constraints of inequation (13) and (14), then the detected lane is verified to be real lane. Otherwise, it is verified to be unreal.

2.4 Calculation of vanishing point

Assume that the parametric equation of line l_i is

$$x\cos\theta'_i + y\sin\theta'_i = \rho_i \quad (15)$$

where θ'_i is the inclination angle and ρ_i is the distance from the origin to the line.

Vanishing point coordinate is represented by (x_M, y_M). Ideally, all the lines in the image intersect at the vanishing point, namely, the sum of the distance from the vanishing point to the line is equal to zero. Thus, the calculation of the vanishing point can be transferred into an extremal problem.

An objective function is constructed in the parameter space:

$$U(x, y) = \sum_{i=1}^{n} (\rho_i - x\cos\theta'_i - y\sin\theta'_i)^2 \quad (16)$$

The vanishing point is the point that makes the objective function obtain minimum:

$$(x_M, y_M) = \arg\min U(x, y) \quad (17)$$

3 Abnormal driving behavior identification

There are two causes of abnormal driving: the direction offset and position offset between the lane and the vehicle. However, the existing ADBIs only focus on one single factor and have poor robustness. Furthermore, they only give out a warning signal and cannot provide specific reason of abnormal driving when abnormal driving occurs.

Fig. 5 shows the condition when the vehicle is traveling straightly at the center of the road. *MA* is the detected left lane and *MB* is the detected right lane. *M* is the calculated vanishing point.

There are two cases of abnormal driving. In the first case, abnormal driving is caused by direction offset.

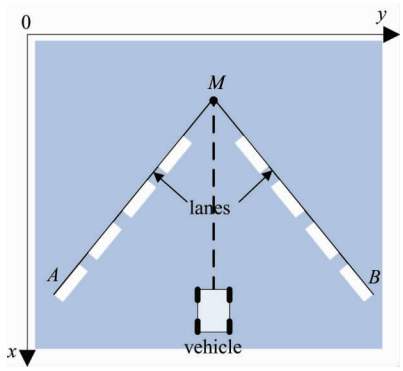

Fig. 5 The schematic diagram of normal driving

Namely, there is an obvious angular offset between the lane and the vehicle. In the second case, the vehicle is going on a straight way, but it is too close to one side of the lane, which is also a potential threat to driving safety.

In order to quantify abnormal driving, two parameters are introduced. β denotes the direction offset between the vehicle direction and line a, which is the angular bisector of the two detected lanes, and l denotes the position offset from the middle of the image to the calculated vanishing point. From Fig. 6 and Fig. 7, it can be found that identifying abnormal driving behavior only by one single factor is unreliable. The reasons are as follows:

(1) In Fig. 6, the thinner lines represent the detected lanes when the vehicle is traveling normally, and the thicker lines represent the detected lanes when abnormal driving caused by direction offset occurs. It is obvious that when abnormal driving caused by direction offset occurs, l can be remarkable while β is still in the normal range shown in Fig. 6.

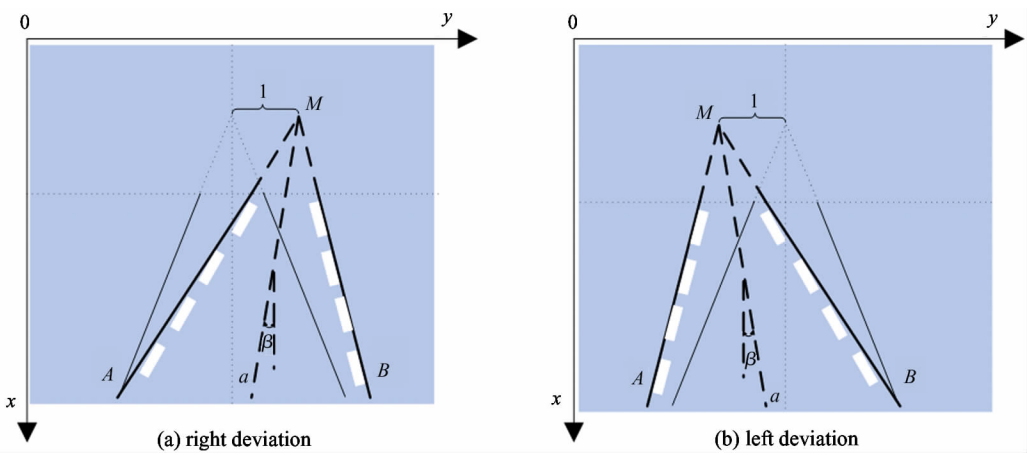

Fig. 6 Abnormal driving situation due to direction biasing

(2) When abnormal driving is caused by position offset, it is β that is in the abnormal scope, but l is within normal limits shown in Fig. 7. Similarly, in Fig. 7, the thinner lines represent the detected lanes

when the vehicle is traveling normally, while the thicker lines represent the detected lanes when abnormal driving caused by position offset occurs.

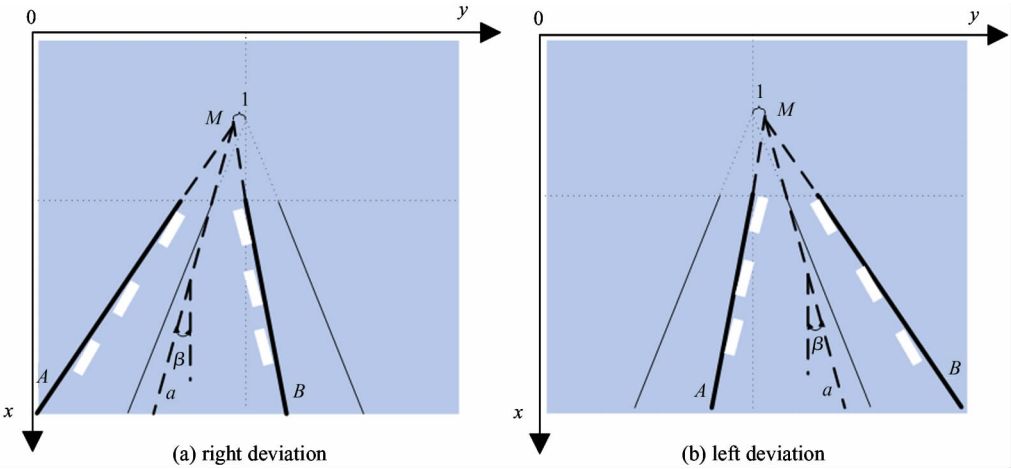

Fig. 7 Abnormal driving situation due to the close distance between the lane and the vehicle

Seen from the above description, when abnormal driving occurs one factor indicates that the vehicle has a tendency to deviate, while another factor is usually still in normal range. Thus, ADBIs which just focus on one single factor are unreliable. Also, there exists obvious difference between normal driving and abnormal driving in the direction offset and position offset. Therefore, in this study, a new ADBI method based on direction and position offsets to improve the reliability of the ADBI is proposed.

The steps of the proposed ADBI are as follows:

(1) If $|\beta| > \beta_T$, where β_T is a set threshold, then abnormal driving caused by direction offset is determined and a warning signal is output directly. Furthermore, if $\beta > 0$, it means the vehicle goes toward left; if $\beta < 0$, it means the vehicle goes toward right. Otherwise, if $|\beta| \leqslant \beta_T$, then turn to the step (2), position offset will be used for further judgement.

(2) If $|l| > l_T$, where l_T is also a set threshold, then abnormal driving caused by position offset is determined and a warning signal is also output. Furthermore, if $l > 0$, it means the vehicle goes toward right; if $l < 0$, it means the vehicle goes toward left. If $|l| \leqslant l_T$, it means the vehicle is traveling normally.

The detailed calculation process of the two parameters, direction offset and position offset, is as follows:

Assume that the linear equations of two detected lanes are $y = k_L x + b_L$ and $y = k_R x + b_R$, the linear equation of the angular bisector can be obtained:

$$y = \frac{k_L + \lambda k_R}{1 + \lambda} x + \frac{b_L + \lambda b_R}{1 + \lambda} \tag{18}$$

where $\lambda = \sqrt{\dfrac{1 + k_L^2}{1 + k_R^2}}$.

Thus, β can be expressed as

$$\beta = \arctan \frac{k_L + \lambda k_R}{1 + \lambda} \tag{19}$$

According to the description above, l represents the position offset from the middle of the image to the calculated vanishing point.

$$l = x_m - x_M \tag{20}$$

where x_m is the abscissa of the middle of the image, and x_M is the abscissa of the detected vanishing point.

The flow chart of the proposed ADBI is shown in Fig. 8.

4 Experimental results

In order to verify the performance of the proposed ADBI method, experiments are conducted in the Nanjing-Zhenjiang expressway, which is 81.7km long. Three men and two women participated in the experiments. Their ages ranged from 22 to 36 years, and they had more than three years of driving experience each. We use an on-board camera to acquire lane images, total 12800 frames of images involving various traffic scenes are used to test the proposed ADBI method.

Some results of lane and vanishing point detection are shown in Fig. 9, where Fig. 9(a) and Fig. 9(b) show the detection on cloudy days, Fig. 9(c) and Fig. 9(d) show the detection at dusk and Fig. 9(e) and Fig. 9(f) show the detection with the interference from other vehicles. Fig. 9(g) shows the result detected on curved road. Fig. 9(h) shows the result detected at night. In Fig. 9, the solid black line represents the detected lane and the black dot represents the calculated vanishing point. Seen from the Fig. 9, although under severe traffic scenes, such as low illuminance at night and occlusion from surrounding vehicles, the proposed method is still able to correctly detect the real

lanes and vanishing points, and the correct rate can reach 97.4%.

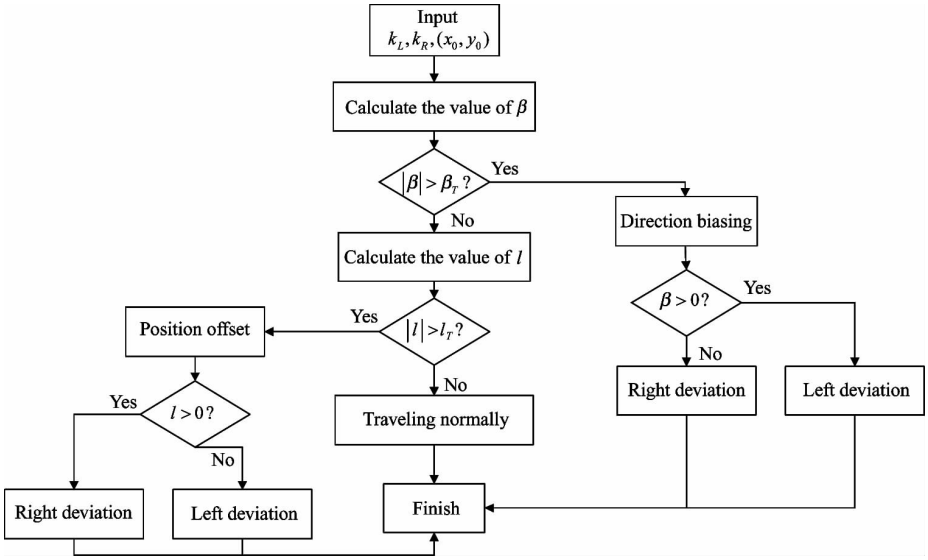

Fig. 8 The flow chart of ADBI

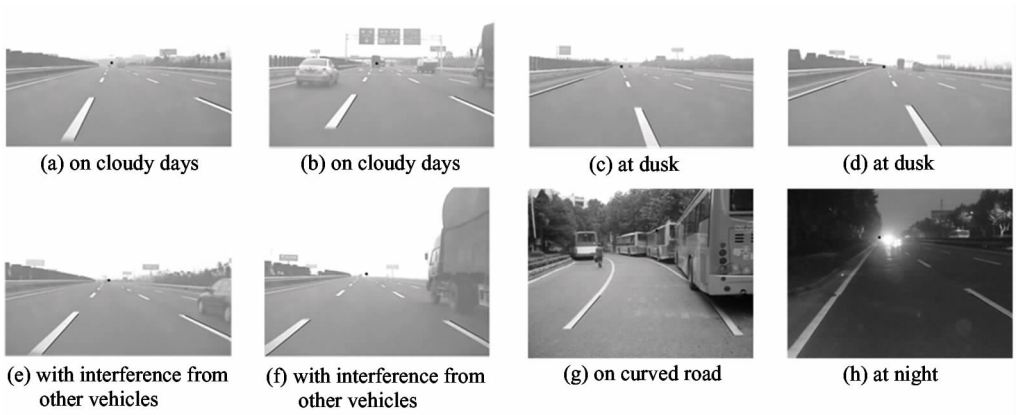

Fig. 9 Experiment of lane and vanishing point detection

Table1 gives out the test results of the proposed ADBI method, where the values of threshold β_T and l_T are related to camera's parameters and the fixed position. In this paper, $\beta_T = 15°$ and $l_T = 50$.

Table 1 Test results of ADBI corresponding to Fig. 9

Number	Left line		Right line		Direction offset	Position offset	Test result
	k_L	α_L (°)	k_R	α_R (°)	β (°)	l (pixel)	
Fig. 9(a)	−0.484	−25.821	2.500	68.199	21.19	--	left deviation (due to direction biasing)
Fig. 9(b)	−0.636	−32.471	2.370	67.122	17.33	--	left deviation (due to direction biasing)
Fig. 9(c)	−3.039	−71.784	0.482	25.747	−23.02	--	right deviation (due to direction biasing)
Fig. 9(d)	−2.883	−70.872	0.728	36.050	−17.41	--	right deviation (due to direcion biasing)
Fig. 9(e)	−0.887	−41.576	2.122	64.767	11.60	27	traveling normally
Fig. 9(f)	−1.228	−50.842	1.788	60.781	4.97	30	traveling normally
Fig. 9(g)	−0.869	−41.000	0.734	36.294	−2.35	−45	traveling normally
Fig. 9(h)	−0.692	−34.700	1.632	58.500	−1.36	61	left deviation (due to position biasing)

Three typical indicators, such as precision, recall, and accuracy, are used to further evaluate performance of ADBI. Their definitions are as follows[13]: precision = $TP/(TP + FP)$, recall = $TP/(TP + FN)$, and accuracy = $(TP + TN)/(TP + FN + FP + TN)$, where, TP, FP, FN and TN are the abbreviations of true positives, false positives, false negatives, and true negatives, respectively.

Experimental results of ADBI under various traffic scenes are shown in Table 2, where "under good scenes" means that the test samples are captured under good illumination or non-occlusion, "under severe scenes" means that the test samples are captured under poor illumination or occlusion from surrounding vehicles.

Compared with state-of-the-art methods[14, 15], the proposed method reaches 97.4% in precision of ADBI. However, the precisions in Refs[14] and [15] are 92% and 90%, respectively. This shows that the proposed method outperforms the state-of-the-art methods.

Table 2 Performance of the proposed ADBI method under various traffic scenes

	Precision (%)	Recall (%)	Accuracy (%)
Under good scenes	97.4	94.7	98.4
Under severe scenes	95.8	92.8	96.3

5 Conclusions

This paper proposes a new ADBI method based on direction and position offsets, where a two-factor identification strategy is used to improve the accuracy and reliability of the ADBI. Self-adaptive edge detection based on Sobel operator is used to extract the edge information of lanes. A Hough transform based on local search scope is employed to quickly detect the lane, and a validation scheme based on priori information is proposed to further verify the detected lane, which enhances the efficiency and reliability of lane detection. Experimental results indicate that the proposed algorithm has strong robustness under complex road conditions.

References

[1] Hu J. Comparison of different features and classifiers for driver fatigue detection based on a single EEG channel [J]. *Computational & Mathematical Methods in Medicine*, 2017, 2017:5109530

[2] Fu R, Wang H, Zhao W, et al. Dynamic driver fatigue detection using hidden Markov model in real driving condition[J]. *Expert Systems With Applications*, 2016, 63(30): 397-411

[3] Jo J, Lee S J, Kang R P, et al. Detecting driver drowsiness using feature-level fusion and user-specific classification[J]. *Expert Systems with Applications*, 2014, 41(4): 1139-1152

[4] Zhao C, Zhang X, Zhang B, et al. Driver's fatigue expressions recognition by combined features from pyramid histogram of oriented gradient and contourlet transform with random subspace ensembles[J]. *IEEE Transactions on Intelligent Transportation Systems*, 2013, 7(1): 36-45

[5] Sandström M, Lampsijärvi E, HolmströmA, et al. Detecting lane departures from steering wheel signal[J]. *Accident Analysis and Prevention*, 2017, 99: 272-278

[6] McDonald A D, Lee J D, Schwarz C, et al. Steering in a random forest: ensemble learning for detecting drowsiness-related lane departures[J]. *Human Factors*, 2014, 56(5): 986-998

[7] Cheng H Y, Jeng B S, Tseng P T, et al. Lane detection with moving vehicles in the traffics scenes[J]. *IEEE Transactions on Intelligent Transportation Systems*, 2006, 7(4):571-582

[8] Feng H, Chen Y, Xu Y. Real-time image acquisition and sobel edge detection based on FPGA[J]. *Transducer and Microsystem Technologies*, 2011, 30(6): 116-118

[9] Yoo H, Yang U, Sohn K. Gradient-enhancing conversion for illumination-robust lane detection[J]. *IEEE Transactions on Intelligent Transportation Systems*, 2013, 14(3): 1083-1094

[10] Yang X, Duan J, Gao D, et al. Research on lane detection based on improved Hough transform[J]. *Computer Measurement &Control*, 2010, 18(2): 292-294, 298

[11] Satzoda R, Sathyanarayana S, Srikanthan T. Hierarchical additive Hough transform for lane detection[J]. *IEEE Transactions on Embedded Systems Letters*, 2010, 2(2): 23-26

[12] Li Q, Wang F, Hu X, et al. A fast lane detection algorithm based on brightness difference[C]. In: Proceedings of the 11th International Computer Conference on Wavelet Active Media Technology and Information Processing, Chengdu, China, 2014. 253-256

[13] Powers D M W. Evaluation: From precision, recall and f-factor to ROC, informedness, markedness &correlation [J]. *Journal of Machine Learning Technologies*, 2011, 2:2229-3981

[14] Xu L, Hu S, Luo Q. A new lane departure warning algorithm consideringthe driver's behavior characteristics [J]. *Mathematical Problems in Engineering*, 2015, 2015: 1-11

[15] Yalic H Y, Keceli A S, Kaya A. On-board driver assistance system for lane departure warning and vehicle detection [J]. *International Journal of Electrical Energy*, 2013, 1(3):132-136

Zhang Xiaorui, born in 1979. She received her Ph. D degree in Instrument Science and Technology Department of Southeast University in 2010. She also received her B. S. and M. S. degrees from Henan University of Science and Technology in 2004 and 2007 respectively. Her research interests include the virtual reality, human-computer interaction, and image processing.